
A HIGH EFFICIENT AND SCALABLE OBSTACLE-AVOIDING VLSI GLOBAL ROUTING FLOW

Junhao Guo
School of Integrated Circuits
Sun Yat-sen University
guojh73@mail2.sysu.edu.cn

Hongxin Kong
Advanced Micro Devices, Inc.
hongxink@amd.com

Lang Feng*
School of Integrated Circuits
Sun Yat-sen University
fenglang3@mail.sysu.edu.cn

March 11, 2025

ABSTRACT

Routing is a crucial step in the VLSI design flow. With the advancement of manufacturing technologies, more constraints have emerged in design rules, particularly regarding obstacles during routing, leading to increased routing complexity. Unfortunately, many global routers struggle to efficiently generate obstacle-free solutions due to the lack of scalable obstacle-avoiding tree generation methods and the capability of handling modern designs with complex obstacles and nets. In this work, we propose an efficient obstacle-aware global routing flow for VLSI designs with obstacles. The flow includes a rule-based obstacle-avoiding rectilinear Steiner minimal tree (OARSMT) algorithm during the tree generation phase. This algorithm is both scalable and fast to provide tree topologies avoiding obstacles in the early stage globally. With its guidance, OARSMT-guided and obstacle-aware sparse maze routing are proposed in the later stages to minimize obstacle violations further and reduce overflow costs. Compared to advanced methods on the benchmark with obstacles, our approach successfully eliminates obstacle violations, and reduces wirelength and overflow cost, while sacrificing only a limited number of via counts and runtime overhead.

Keywords Physical design, Global routing, Obstacle-avoiding rectilinear steiner minimal tree

1 Introduction

Routing is a crucial step in the back-end design of very large-scale integrated circuits (VLSI). It consists of two main phases: global routing and detailed routing. Global routing focuses on generating routing paths for every net to optimize performance and minimize violations as much as possible. In contrast, detailed routing addresses and resolves any violations after the global routing phase. The quality of global routing significantly impacts the workload of detailed routing and the overall performance of the circuit. Furthermore, improvements in global routing can often be achieved more easily with advanced algorithms. Consequently, both academia and industry have invested substantial efforts in developing fast, scalable, and robust global routing engines.

As the number of cells and nets in modern designs has increased dramatically in advanced technology, more complicated obstacles have emerged in global routing to accommodate more complex functionality requirements or to maintain consistency with earlier design phases. These obstacles may arise from various sources, including macro cells, intellectual property (IP) blocks, 3D packaging, pre-routed nets, power networks, etc. However, many global routers struggle to efficiently handle obstacle information and generate obstacle-free solutions at the global routing phase. High-efficiency obstacle-avoiding global routing has become more challenging and more necessary than ever before.

Global routing typically involves several steps, including tree generation, initial routing, and rip-up and reroute phases. Traditional routers that lack specialized methods for avoiding obstacles typically generate rectilinear Steiner minimal trees (RSMTs) for nets, which can be quickly obtained using established algorithms like FLUTE [1]. Without full consideration of obstacles, numerous design-rule violations can occur in the solutions. Although these violations

*Corresponding author

can be addressed in later stages, with more time-consuming algorithms like maze routing, the overall efficiency and effectiveness of the routing process can become limited. To address the obstacle-avoiding RSMT (OARSMT) problem, recent research has introduced several algorithms for single-net solutions, such as complex graph algorithms, machine learning, etc. With more complex obstacle distributions, the complexity can significantly increase, especially for high fan-out nets. Additionally, the number of nets has also risen dramatically in modern designs. These result in scalability problems for most OARSMT algorithms in practicality when applied to large-scale cases in global routing. As a result, most of the previous researches primarily concentrate on the tree generation phase and lack a comprehensive obstacle-avoiding global routing flow.

In this article, we present an efficient and scalable obstacle-avoiding global routing flow using the proposed rule-based OARSMT algorithm for initial routing, along with OARSMT-guided and obstacle-aware sparse maze routing for the rip-up and reroute process. These methods successfully generate valid solutions under different distributions of obstacles in large designs, demonstrating high efficiency. The main contributions of this article are as follows:

- We propose a global routing flow using the proposed rule-based OARSMT algorithm to avoid obstacle violations at the early stage. This is followed by two obstacle-aware rip-and-reroute approaches, ultimately generating an obstacle-free solution for every net.
- We propose a rule-based OARSMT algorithm that utilizes multiple rule-based schemes to enhance the results from FULTE and operates very quickly. With its high scalability, it can address most obstacle violations for all nets in a complete design during tree generation.
- An OARSMT-guided sparse maze routing is proposed, which is guided by the OARSMT structure generated in the initial routing. This significantly decreases obstacle violations and overflow during rip-up and reroute processes. Additionally, an obstacle-aware sparse maze routing technique is introduced to manage particularly hard-to-route nets.
- The proposed obstacle-avoiding global routing eliminates obstacle violations while delivering a 1.96% improvement in wirelength and a 28.06% reduction in overflow cost on ISPD24 benchmarks with various obstacles, with limited via count and runtime overhead. Furthermore, The proposed OARSMT algorithm achieves a significant $\sim 10x-2700x$ and $\sim 150x-5800x$ runtime speedup compared to advanced OARSMT algorithms on randomized testcases and standard OARSMT benchmarks, respectively, with minimal wirelength overhead.

The remaining of this article is organized as follows: In Section II, a brief background and formulation on global routing and OARSMT is presented. In Section III, a brief introduction to our obstacle-avoiding global routing flow is proposed. In Section IV, the exact OARSMT algorithm in detail is described. In Section V, the details of our obstacle-avoiding global routing, including initial routing and rip-up and reroute, are presented. In Section VI, the experimental evaluation is discussed. Finally, in Section VII, the main conclusion is drawn.

2 Background

2.1 Related Work

OARSMT Generation: OARSMT problem has been researched for many years. In the last century, the work [2] proposed the approach to calculate the shortest connection between two pins in a layout with obstacles. Recently, with the increasing constraints in new technologies, OARSMT becomes more important. For example, work [3] first constructs an RSMT without considering obstacles, and then uses a four-step algorithm to legalize the edges that intersect with the obstacles. However, the scenarios of the legalization is relatively straightforward and does not globally consider enough conditions. Work [4] proposes a solution using the obstacle-avoiding spanning graph (OASG), which trims edges and nodes to yield a minimum spanning tree for an acceptable quality OARSMT in polynomial time. However, it may overlook optimal solutions early on, resulting in excessive wirelength, and has impractical runtimes for complex cases. In contrast, work [5] also utilizes OASG but incorporates FLUTE for fine-tuning, achieving better quality and runtime, however it misses early global guidance from FLUTE. Work [6] approaches the OARSMT problem using the λ -geometry plane. Subsequent works [7, 8, 9, 10, 11] address multi-layer OARSMT, with work [11] being high quality by leveraging intermediate information of maze routing to optimize tree costs, reducing runtime while improving quality. Additionally, work [12] explores machine learning, employing a reinforcement learning algorithm to generate tree structures for small cases (12 pins, 20 obstacles) within limited runtimes. Compared with the previous works, leveraging the predefined rules, the proposed OARSMT algorithm has overall better quality, and has limited runtime, especially in large cases.

Global Routing: Global routing is one of the critical steps in physical design, and there are many studies investigating efficient global routing. For example, FastRoute 1.0 [13] constructs a steiner tree based on congestion cost, further

reducing congestion through edge-shift techniques, and ultimately achieves a high-quality solution by maze routing algorithms. FastRoute 4.0 [14] leverages the via aware steiner tree generation, 3-bend routing and layer assignment to reduce the via count and runtime. NTHU-Route [15] utilizes iterative rip-up and reroute with innovative techniques to improve routing efficiency. To enhance solution quality and runtime performance, NTHU-Route 2.0 [16] incorporates a new history-based cost function, new ordering methods for congested region identification and two implementation techniques. FGR [17] utilizes 3D maze routing based on discrete Lagrange multipliers to reroute net for an existing routing solution, GRIP [18] leverages integer linear programming to choose an optimal route for each net. These two methods run too slowly to be practical. MGR [19] resorts to an efficient multi-level framework to reroute nets in the congested region on the 3D grid graph with comparable runtime of 2D. Recently, CUGR 2.0 [20] uses DAG-based 3D pattern routing and sparse grid graph maze routing. Compared to majority routing algorithms, CUGR 2.0 not only demonstrates a substantial improvement in the quality of results but also significantly reduces the running time, showcasing enhanced computational efficiency. However, the above mentioned methods have not specifically considered the wide presence of obstacles with arbitrary numbers and sizes, leading to inefficiency of solving the violations by the obstacles.

To address the aforementioned issues, we propose a novel obstacle-avoiding global routing flow. This flow involves using our proposed fast and efficient OARSMT algorithm during the initial routing phase, and employing OARSMT-guided sparse maze routing and obstacle-aware sparse maze routing during the rip-up and reroute phase. Experiments indicate that this flow is effective when obstacles are widely involved.

2.2 Problem Formulation

In 3D global routing, the layout area is typically partitioned into an array of rectangular cells called global routing cells (GCells), which is represented as a 3D grid graph $G(V, E)$. Each GCell is treated as a vertex ($v \in V$). A complete input case C consists of lots of nets, with each net containing m pins $\{p_0, p_1, p_2, \dots, p_{m-1}\}$. Besides, there are n obstacles $\{b_0, b_1, b_2, \dots, b_{n-1}\}$ that are all rectangles with width w_i and height h_i for each b_i . The OARSMT problem and the global routing problem based on the obstacle-avoiding feature are defined as follows.

The OARSMT problem used in global routing tree generation is to find a rectilinear steiner tree with minimal wirelength that connects all pins, with no edge crossing any obstacles and no steiner node located inside any obstacles. The pins and obstacles are located in a xy -plane without overlap. Therefore, when executing OARSMT, it is necessary to map the obstacles in 3D space to 2D space. The cost of the tree is the wirelength, and an edge passing through (or a steiner node located at) the boundary of an obstacle is assumed to be legal.

For the complete global routing problem with obstacles, the capacity of an edge between a GCell represents the number of available routing tracks through it. The demand of an edge represents the capacity that has already been used on that specific edge. In the event where the demand of an edge exceeds its capacity, it leads to an overflow. It is established that obstacles are not traversable by route of net. As a consequence, the capacity of the area where obstacles are positioned is rendered as zero. The primary objective of obstacle-avoiding global routing is to minimize the $cost(C) = WL + \alpha_{ow}OW + \alpha_{ov}OV$, where WL is the total wirelength of all nets, OW is the total overflow cost, and OV is the cost of obstacle violations. Note that since an obstacle is not traversable, its violation weight α_{ov} is high enough.

3 Proposed Global Routing Flow Overview

The proposed global routing flow avoids obstacles during routing with obstacle-aware tree generation and two stages of maze routing. These steps are illustrated in Figure 1. The key steps highlighted in gray are explained in more detail below.

(1) *OARSMT Generation*: To minimize the number of net connections obstructed by obstacles during the initial routing, we construct an OARSMT in the tree generation stage. The OARSMT algorithm begins by using the FLUTE algorithm to determine the structure of the Rectilinear Steiner Minimum Tree (RSMT). Then, the algorithm updates the steiner nodes and edges that intersect with obstacles using a very fast newly proposed rule-based method, and completing the OARSMT generation. Then an initial route of the net is obtained in pattern routing. Compared to traditional initial routing methods, the proposed approach demonstrates a significant reduction in the number of nets that encounter obstacles, all while maintaining high processing speeds. This improvement can improve the subsequent obstacle-avoiding processes and offer valuable guidance for the later stages of routing.

(2) *OARSMT-Guided Sparse Maze Routing*: Although the number of nets with obstacle violations has significantly improved after initial routing, there are still many overflow issues and some violated nets. We propose a method called OARSMT-guided sparse maze routing. This method utilizes the OARSMT structure generated during the initial routing

as a guide. It incorporates relevant paths into a sparse graph and performs maze routing within this graph. Compared to traditional sparse maze routing, our approach has a higher likelihood of avoiding obstacles, effectively reduces overflow, and achieves a speed comparable to that of standard sparse maze routing.

(3) *Obstacle-aware Sparse Maze Routing*: If there are still nets that have not successfully avoided obstacles, we will perform more refined maze routing for these nets called obstacle-aware sparse maze routing in this study. The obstacle-aware sparse grid graph will be constructed first, incorporating the boundaries of all obstacles, and maze routing will be performed within this graph. After this phase, the vast majority of nets can successfully navigate around obstacles.

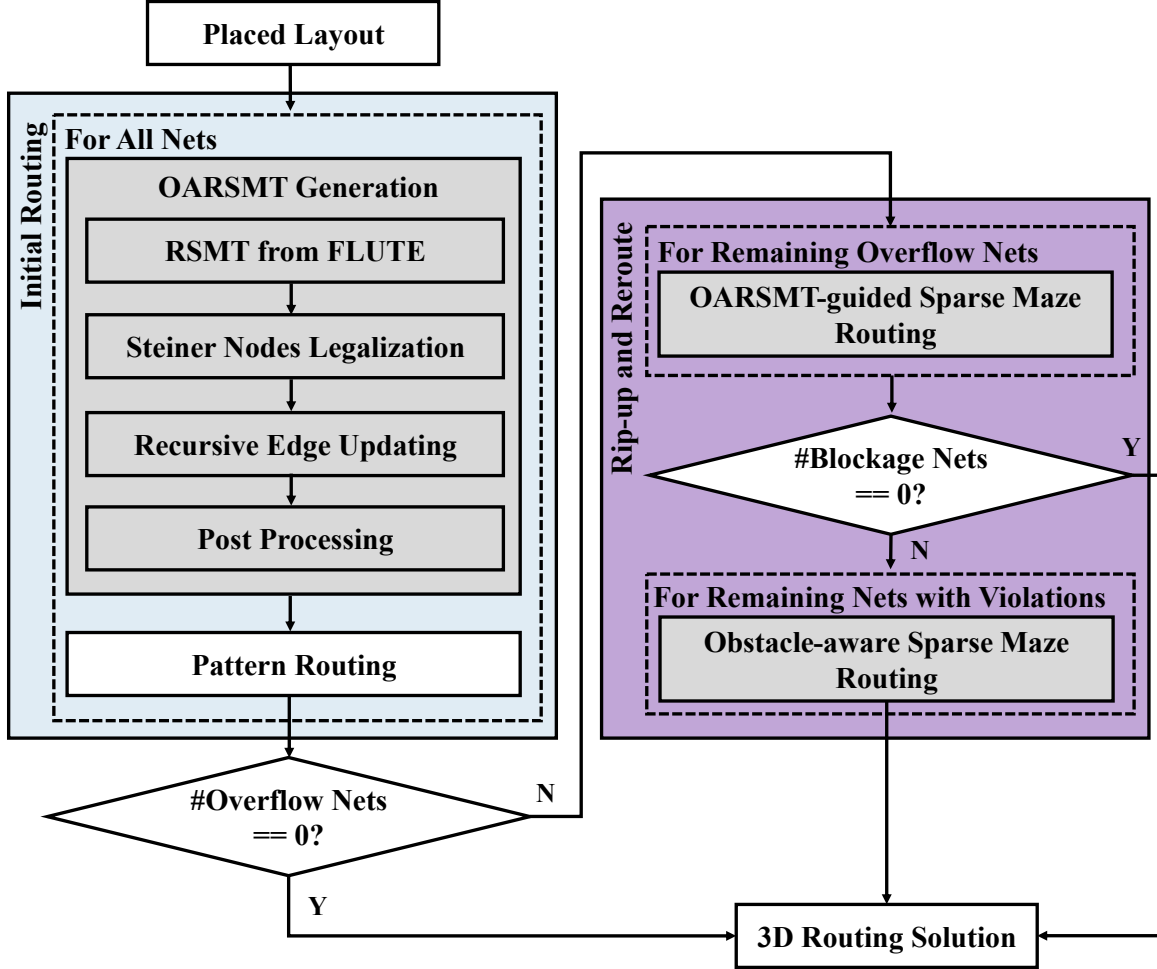


Figure 1: The proposed routing flow. (The proposed algorithms are shown as gray rectangles.)

4 OARSMT Algorithm Design

The first key process is the OARSMT generation during the initial routing. With great amount of nets, the proposed OARSMT algorithm can quickly generate the tree structures that avoid the obstacles. The generated OARSMTs can reduce the obstacle violations at the early step, which can release the workload of later steps and provide guidance for maze routing for better quality and runtime. In the following subsections, the design rationale of the proposed OARSMT algorithm is introduced, then the detailed algorithm and flow are elaborated.

4.1 Design Rationale and Edge Updating

As FLUTE does not consider obstacles, previous OARSMT works do not apply it in the early stage. This may leave out the valuable guidance of optimized tree structures, and incur more runtime. The proposed algorithm in this work

leverages the solutions of FLUTE as a guidance, and further updates the solutions to optimize and legalize the layout with obstacles.

The basic procedure to perform the solution updating is to find all the straight-line edges from a FLUTE solution that cross obstacles, and update them one by one. Using maze routing or recording the patterns of obstacles in a look-up table might be two approaches, but they either suffer from large runtime or tremendous patterns to be recorded. A trade-off approach can be the rule-based edge updating. Two example rules to update the edges from FLUTE are shown in Figure 2(a), including directly detouring the obstacles, and connecting through the obstacle boundaries. However, they can incur large cost or even violations with other obstacles, indicated as red lines in Figure 2(a).

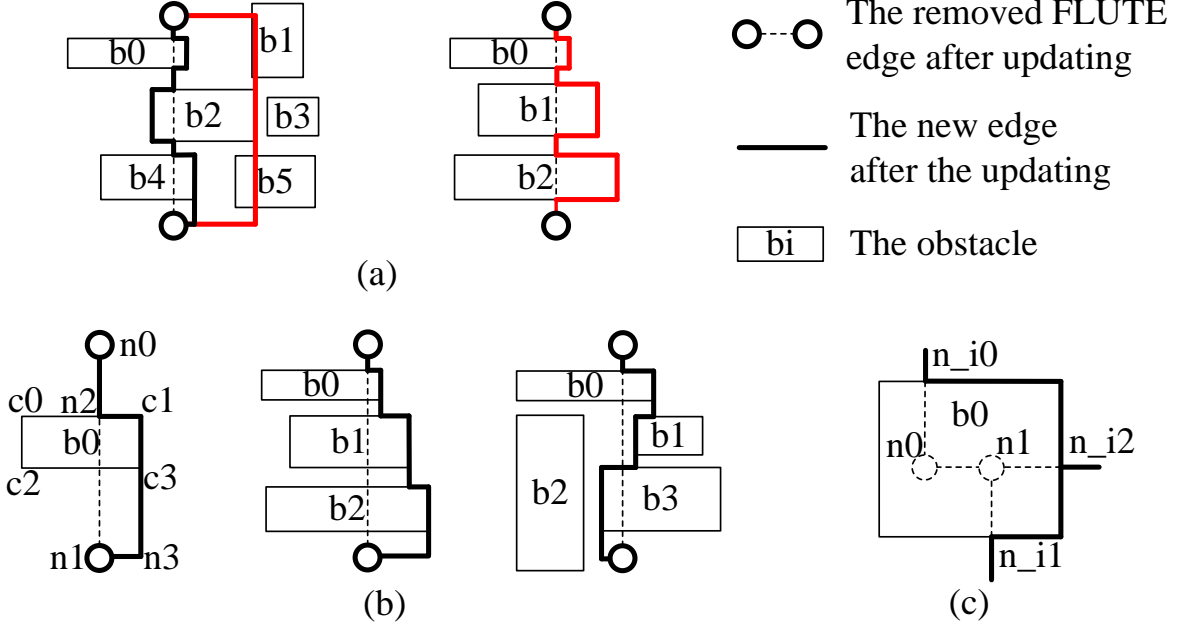


Figure 2: (a) Examples of directly detouring and connecting through the obstacle boundaries; (b) The examples where the proposed reference line-based edge updating show the optimal solutions; (c) An example where the steiner nodes generated by FLUTE are in an obstacle.

To tackle the above challenges while keeping the fast process, a new rule-based edge updating approach is proposed, which keeps a balance between the two rules in Figures 2(a).

In short, the new algorithm iteratively bends the edge line only when it is blocked on its direction, and each time bends to the obstacle corner nearest to the original edge. Taking the left part of Figures 2(b) as an example, the line of the original edge generated by FLUTE is named the *reference line* (such as $[n_0, n_1]$). One of the nodes of the original edge is first selected as the source node (such as n_0), while another is the target node (such as n_1). The direction from the source node to the target node is named the *reference direction*, which is vertically from the top to the bottom in this example. Then, a line is created and extended from the source node to the target node through the reference direction. Once the line is blocked by an obstacle’s boundary (e.g., the line extended from n_0 is blocked at n_2 by the top boundary of b_0), it is bent and extended to a corner of this boundary (e.g., the extended line segment after bending is $[n_2, c_1]$). The direction of bending is to the corner that is closer to the reference line (e.g., corner c_1 in this case). Once the bent line is extended and reaches the obstacle’s corner, it is then bent again and extends through the reference direction again (such as $[c_1, n_3]$). Once the line is extended to have the same coordinate as the target node (e.g., n_3 has the same y-coordinate as n_1), the line is bent again towards the target node and connects it.

Except the edge itself, the steiner nodes from FLUTE on edges also need to be updated when they are located inside the obstacles, such as the example in Figure 2(c). This can be fixed by regenerating the edges shown as the black lines in the figure, and removing the invalid edges and nodes. The black lines are generated as the shortest edges placed around the obstacle that can connect all the intersection points ($n_{i0}-n_{i2}$).

4.2 Rule Enhancements

(1) *L-Shape Optimization*: Although the edge updating performs well for the cases in Figure 2, there are still some cases that are difficult with only the basic edge updating. For example, In Figure 3(a), 3 steiner nodes from FLUTE

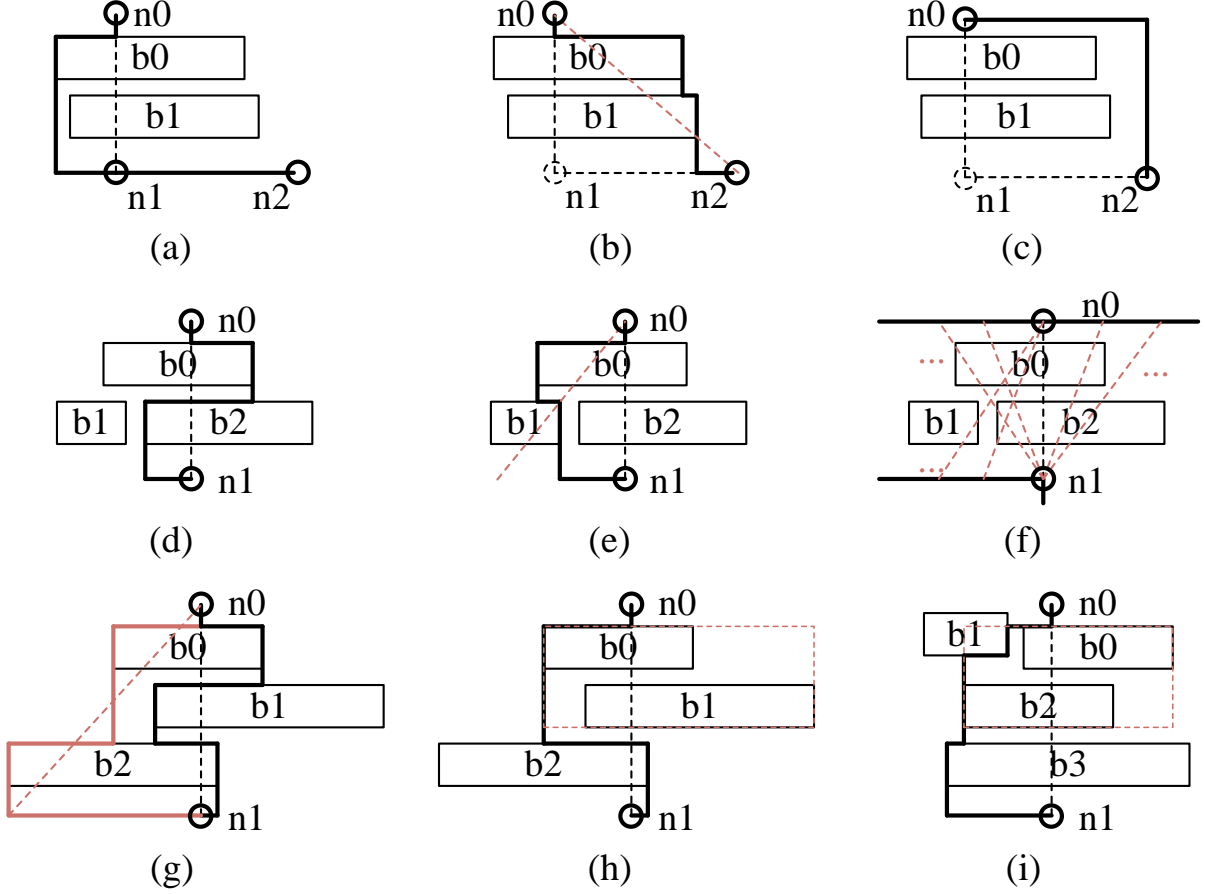


Figure 3: (a)-(c) An example of better-updating L-shape connections. (d)-(f) An example of the benefit by sloping the reference line. (g)-(i) An example of the benefit by merging obstacles. (The reference line is shown as the red dotted line if it is not overlapped with the original edge to be updated, and the red solid lines are the its corresponding updated edges, if illustrated.)

are shown. Edge updating needs to update $[n_0, n_1]$, and the solution is Figure 3(a) as the left corner of b_0 is nearer to $[n_0, n_1]$. However, if n_0 connects n_2 by the edges on the right of Figure 3(b), after $[n_0, n_1]$ and a segment of $[n_1, n_2]$ are removed, the optimal solution can be obtained. This can be realized by setting the reference line as $[n_0, n_2]$. Besides, if we change the L-shape direction as Figure 3(c), another optimal solution can also be obtained. Inspired by these findings, given an edge $[n_i, n_j]$ needs to be updated, if the degree of n_i or n_j is 2 (which means there exists an L-shape), the reference line of edge updating is the diagonal of this L-shape. Besides, two types of L-shapes are both tried to perform the edge updating, and the solution with a smaller wirelength is kept.

(2) *Reference Line Sloping*: Besides for L-shapes, there are also other cases that can be explored. For example, Figure 3(d) shows the solution of the proposed edge updating for $[n_0, n_1]$, but a better solution is shown in Figure 3(e). This can be obtained by setting the reference line with a slope to the left. Therefore, when updating $[n_i, n_j]$, all its orthogonal half-lines (at most 4) starting from n_i (or n_j) are considered to build the reference lines between the source node n_j (or n_i) and a node on the half-lines, respectively. k_l evenly distributed reference lines within the bounding box are tried for each half-line, where k_l is set by users. An example is shown in Figure 3(f). After updating edge $[n_0, n_1]$ by multiple reference lines, the solution with the smallest wirelength is kept.

(3) *Obstacle Merging*: Another approach for rule enhancement is to merge multiple nearby obstacles, and the bounding box of these merged obstacles is regarded as a new obstacle when applying edge updating. In Figure 3(g), the original edge updating incurs large cost due to lots of bends, and the sloped reference line on the left can also incur large cost. In contrast, the solution in Figure 3(h) becomes more optimized where b_0 and b_1 are merged. Note that sometimes merging obstacles can cause overlaps, such as b_1 in Figure 3(i). Considering the runtime, if the edge updating is blocked by the overlapped obstacles, the edge extends on the boundaries of the overlapped obstacles, through the shortest path until able to perform the edge extension without the overlaps. Finally, similar to the reference line sloping approach, when updating each edge $[n_0, n_1]$, k_m merging strategies are tried, where k_m is set by users. More specifically, if there

Algorithm 1 Rule-based OARSMT algorithm**Function:** OARSMT_Generation**Input:** Pins S_p ; Obstacles S_b .**Output:** Edges that connect all pins S_e .

```

1:  $S_{Fe} \leftarrow$  Run FLUTE to get the solution of edges
2:  $S_e \leftarrow$  Build the rectilinear tree based on  $S_{Fe}$ 
3: for Each obstacle  $b$  in  $S_b$  do
4:    $S_n \leftarrow$  The set of nodes locating inside  $b$ 
5:   Revise edges in  $S_e$  related to  $S_n$ .
6: end for
7: for Each edge  $e$  in  $S_e$  do
8:    $S_{be} \leftarrow$  The set of obstacles that blocks  $e$ 
9:   if  $S_{be} == \emptyset$  then
10:    Continue
11:  end if
12:   $B_b \leftarrow$  The bounding box of all obstacles in  $S_{be}$ 
13:   $S_{candb} \leftarrow$  The set of obstacles that overlap  $B_b$ 
14:   $U_{emin} \leftarrow \emptyset, WL(U_{emin}) \leftarrow \infty$ 
15:  for Each merging strategy solution  $S_{mb}$  of  $S_{candb}$  do
16:    for Each possible  $l_r$  and source node  $n_s$  of  $e$  do
17:       $U_e \leftarrow$  Edge_Update( $n_s, l_r, S_{mb}$ )
18:      if  $WL(U_e) < WL(U_{emin}), U_{emin} \leftarrow U_e$ 
19:    end for
20:  end for
21:   $S_e \leftarrow S_e \setminus e$ 
22:   $S_e \leftarrow S_e \cup U_{emin}$ 
23: end for
24: Remove redundant edges, merge overlapped edges in  $S_e$ 
25: Return  $S_e$ 

```

are n' obstacles that cross $[n_0, n_1]$, the merging strategies of merging each 1, n'/k_m , $2n'/k_m$, $k_m \times n'/k_m$ obstacles are tried, and the solution with the smallest wirelength is kept.

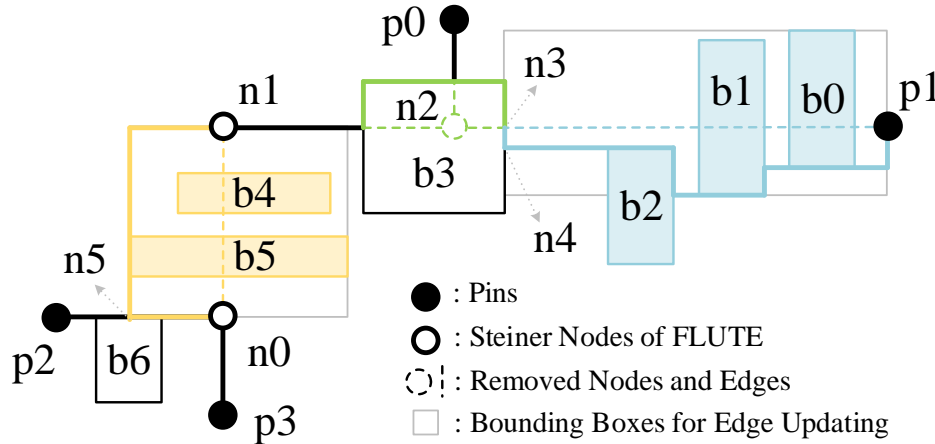
4.3 The Rule-Based OARSMT Algorithm

Figure 4: An example of the solution from the proposed algorithm. (Different colors stand for different elements considered in different processes)

Based on the edge updating rule, the proposed rule-based OARSMT algorithm is proposed in Algorithm 1, where the inputs include a set of pins S_p and a set of obstacles S_b . It outputs a set of edges S_e as the solution. The flow can be separated into 4 steps.

(1) *RSMT Generation*: For the first step, the FLUTE solution is obtained (Line 1 of Algorithm 1). This solution usually only includes the connections between nodes, and thus a rectilinear tree first needs to be built as S_e in Line 2. Each edge between two connected nodes from FLUTE is constructed by an L-shape pattern, and the direction is basically randomly selected at first.

(2) *Steiner Nodes Legalization*: The second step is to legalize the steiner nodes inside the obstacles (Lines 3-6) as Figure 2(c). For a set of invalid steiner nodes S_n within an obstacle b , the intersection points between b 's boundaries and edges connecting nodes in S_n are found. Then, the shortest edges placed around the obstacle boundaries that are able to connect all such intersections are calculated and added to edge set S_e . Finally the edge segments inside b are removed from S_e . An example is also shown as the green parts in Figure 4.

(3) *Iterative Edge Updating*: The critical step is edge updating, which is iteratively performed (Lines 7-23). Each time an edge e with violations is selected, the set of obstacles S_{be} that block e is obtained (Line 8). Then, a bounding box B_b is heuristically introduced to greatly reduce the complexity (Line 12). The bounding box is a rectangle that just surrounds e and all obstacles in S_{be} , and the candidate obstacles S_{candb} are selected as the obstacles overlap B_b (Line 13). For example, in Figure 4, when updating edge $[n_0, n_1]$, B_b is built based on $[n_0, n_1]$, b_4 and b_5 . In this case, $S_{candb} = \{b_4, b_5\}$. In contrast, when updating edge $[p_1, n_3]$, although B_b is not built based on b_2 , but b_2 is included in S_{candb} since B_b overlap b_2 . Next, a record of the minimum wirelength connection is initiated at Line 14, and the edge updating by all combinations of approaches introduced in Sections 4.1 and 4.2 is performed to e (Lines 15-16), with the consideration of the obstacles in S_{candb} . After this, the merged obstacles S_{mb} , a reference line l_r and a source node n_s is selected, and the edge updating is performed (Line 17). Once a solution with better wirelength is found, the record U_{emin} is updated (Line 18). The best solution is selected to replace edge e (Lines 21-22). Note that all updated new edges will be further checked after edge updating of e , as they might also cross obstacles, so finally all edges are legal.

(4) *Post Processing*: Finally, each edge connecting a steiner node with degree 1 is removed, and the overlapped edges are merged (Line 24). This can be finished quickly by checking the edges connected to each steiner node or pin. Additionally, we perform cycle detection on the generated tree. Even if a non-tree structure is produced, it can be quickly repaired using classical algorithms. In our experiments, the probability of generating a non-tree structure is $\sim 1\%$.

4.4 Data Structure Improvement and Time Complexity

The critical and the most time-consuming part is the iterative edge updating (Lines 7-23 in Algorithm 1). During this part, frequently checking for if a line crosses any obstacles (and which obstacles) is needed, such as by Line 8 of Algorithm 1, especially when bending an edge during the edge updating in Section 4.1. This can be realized by using an R-tree to store obstacles and querying it to check if a segment or rectangle overlaps with any obstacles. However, the R-tree structures are relatively complex and general that also allow the insertions and overlaps of the stored rectangles (obstacles). As obstacles are typically fixed and can be represented by non-overlap rectangles, the R-tree data structure can be replaced by simpler data structure for higher efficiency. Therefore, we propose a specific data structure to avoid redundant functions and it is illustrated in Figure 5. For example, Figure 5 shows a layout with obstacles indicated as gray rectangles. The Hanan grid can then be generated as the dotted lines. Note that the grid is not only based on the pins and the boundaries of obstacles, but also based on the centers of obstacles such as k_{b_3} of b_3 . For each row and column of the grid, a *range list* is maintained with multiple sorted pairs of numbers, separated by semicolons. Each pair is a range of an obstacle's width or height, respectively. We name each pair as *range pair*. For example, for Row 1 ($y = 1$), there are two obstacles b_0 and b_1 , which are located at $0 \leq x \leq 3$ and $4 \leq x \leq 5$, respectively. In this case, two range pairs are stored as $\{0, 3; 4, 5\}$. Besides, to track which obstacle each range pair corresponds to, additional lists containing the obstacle pointer for each range pair are maintained, which is not shown in this example. The range lists are built in $O(n)$ runtime for one time, by checking the locations and ranges of all obstacles and pushing the ranges into the corresponding list.

After the range lists are built, checking which obstacles a given line crosses can be quickly finished. The procedure can be illustrated by checking the line e in Figure 5. e is horizontally located at Row 2, so the x-coordinates (1 and 6) of e 's two nodes n_0 and n_1 are checked in the range list $\{0, 3; 4, 5; 7, 8\}$ to obtain the list indices where these two x-coordinates are. n_0 locates between $x = 0$ and $x = 3$ (between indices 0 and 1 of $\{0, 3; 4, 5; 7, 8\}$), while n_1 locates between $x = 5$ and $x = 7$ (between indices 3 and 4). The obstacles of which the range pairs' indices are between the indices of n_0 's and n_1 's locations are categorized as crossed the line e . In this example, the obstacles cross e are b_0 and b_1 . The obstacles can be obtained by the maintained obstacle pointers associated with the range pairs. The checking only needs $O(\log(n))$, since each list is sorted and contains at most all n obstacles' ranges.

Furthermore, if all obstacles that a bounding box (such as B_b in Figure 5) overlap need to be obtained, a short boundary of the bounding box ($[c_0, c_1]$) can be selected, and each grid line orthogonal to the short boundary inside

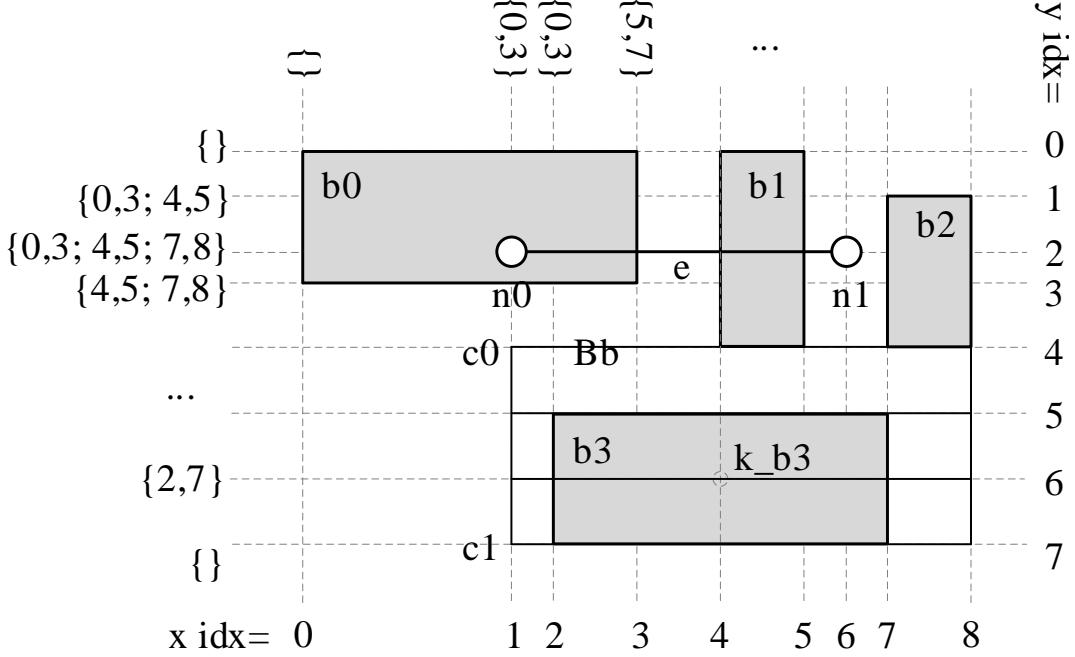


Figure 5: An example of the improved data structure. (The grids based on the centers of obstacles are not completely shown in this example for more clearly illustrating. Only the center k_{b_3} of b_3 is shown.)

B_b is then selected, which is shown as the 4 horizontal lines in B_b (including 2 long boundaries and the line through the center of b_3). Finally, these selected lines are iteratively checked to get all overlapped obstacles. The runtime is $O(len_{minb} \times \log(n))$, where len_{minb} is the length of the short boundary of the bounding box.

Based on this, the overall time complexity is analyzed as follows. The main time-consuming part is edge updating. Since an edge at most crosses n obstacles, the bending of the edge performs at most n times. Each time an edge is bent, the crossed obstacles need to be checked and the first one to the source node is selected, so it needs $O(n \log(n))$ runtime in total for each edge updating. When k_l for reference line sloping and k_m for obstacle merging are globally fixed in the tool for any layouts as in our experiments, it does not affect the time complexity. In Algorithm 1, as there are m pins, the order of the edges in S_e from FLUTE is $O(m)$. This infers that Lines 7-23 basically perform $O(m)$ times. As Lines 8, 12, and 17 needs $O(\log(n))$, $O(len_{minb} \log(n))$, and $O(n \log(n))$ runtime, the overall time complexity is $O(m \times (\log(n) + len_{minb} \log(n) + n \times \log(n)))$. In practice, usually the maximum size of the support layout for a placer is fixed, so len_{minb} is a constant. In this case, the time complexity is $O(m \times n \times \log(n))$. This is less than the state-of-the-art previous work [11]. Besides, in most cases, an edge crosses only a small portion of obstacles, and the n in the time complexity is much smaller than the number of all obstacles. This further leads to fast speed in practice.

5 Obstacle-Avoiding Global Routing

Based on the proposed OARSMT algorithm, the obstacle-avoiding global routing flow in Section 3 is elaborated.

5.1 Initial Routing

Global routers often overlook obstacles during initial tree generation, leading to violations. The upper diagram of Figure 6(a) shows the solutions generated for four multi-pin nets without considering obstacles. This oversight significantly burdens the subsequent phases. In the initial routing stage that we propose, we take into account obstacles during the routing process. By employing the efficient OARSMT algorithm during tree generation, we can greatly reduce the instances of obstacle violations in the initial routing phase while ensuring speed is maintained, as shown in Figure 6(a).

The first step of initial routing is to generate OARSMTs for all nets. To reduce runtime while maintaining quality, the OARSMT algorithm only considers obstacles that overlap with the bounding box of each net as part of its inputs. This may result in some nets being violated, but these issues can be quickly addressed in subsequent steps. After generating the OARSMTs for all nets, traditional pattern routing is applied to determine the routing patterns and the layers of the

edges. An example of pattern routing with layer assignment is illustrated in Figure 6(b) and (c), which also presents the initial routing solution.

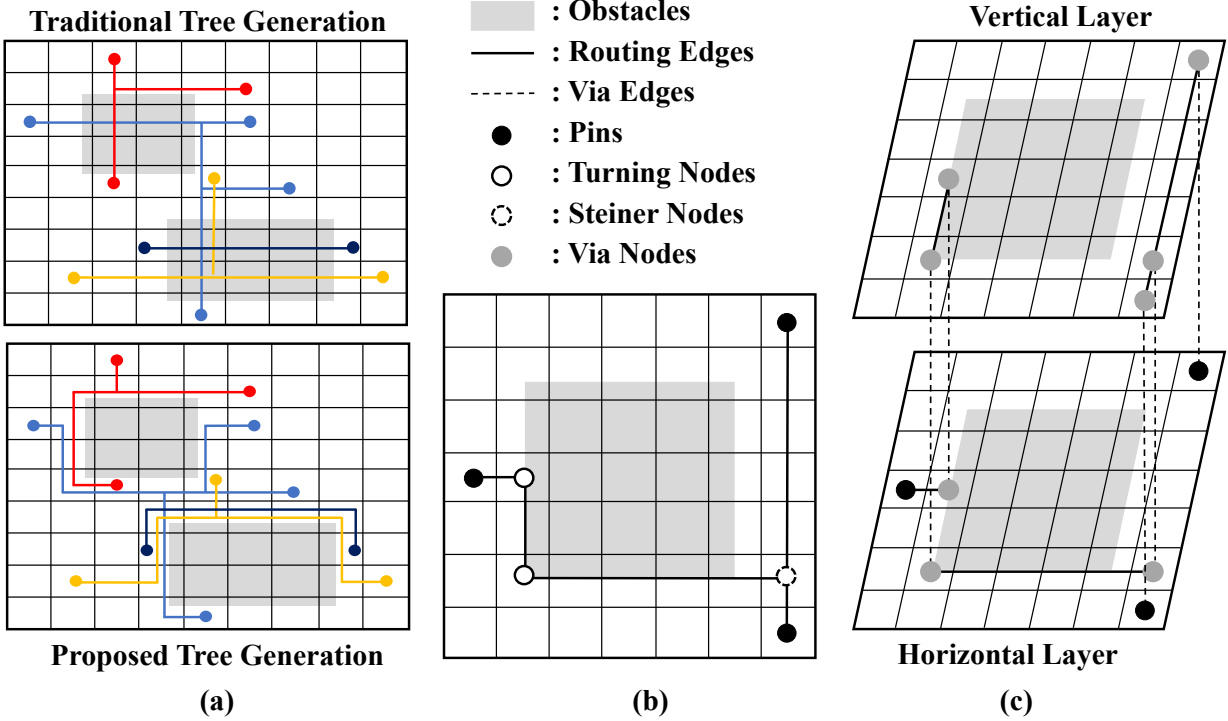


Figure 6: (a) An example of a simple case corresponds to both traditional initial routing and our proposed initial routing. The different colors represent different nets. (b) An example of the 3D result obtained under our initial routing. (c) The corresponding 2D solution of (b).

Note that although the proposed approach in Figure 6(a) places more demands and bends on GCells near obstacles than the traditional one due to the avoiding of obstacles by OARSMTs, it does not infer that the proposed approach incurs greater congestion, as the traditional approach does not even begin to effectively avoid obstacles at this stage. Actually, the proposed approach has even less congestion in the final results, because most of the obstacles are already well avoided at the very early stage, which alleviates the tasks during rip-up and reroute.

5.2 Rip-up and Reroute

Although initial routing can help most nets avoid obstacles, further attention is needed to address congestion. Therefore, maze routing is applied to rip-up and reroute the remaining overflowed and violated nets. However, maze routing is time-consuming due to the extensive search space involved. One relatively effective method to reduce the search space for maze routing, without significantly compromising solution quality, is to use sparse graphs. Unfortunately, in many cases, the paths generated on a sparse graph may not provide obstacles-avoiding solutions, as illustrated in Figure 7(a) and (d). To remedy this, we propose OARSMT-guided sparse maze routing and an enhanced obstacle-aware sparse maze routing approach, both of which significantly improve the likelihood of avoiding obstacles while maintaining limited runtime overhead.

(1) *OARSMT-Guided Sparse Maze Routing*: In order to significantly reduce overflows while eliminating obstacle violations during the rip-up and reroute phase, we propose OARSMT-guided sparse maze routing in the first stage of rip-up and reroute. During the process of rip-up and reroute for each net, additional sparse grid lines are created by utilizing the OARSMT structure established during the initial routing. These grid lines extend from each edge of the OARSMT and have a specific width. An example is shown as blue lines in Figure 7(b), which follow the extension of the dotted lines. By combining the ordinary sparse graph and the additional grid lines, the OARSMT-guided sparse graph is generated. An example is shown in Figure 7(c). When performing maze routing on the generated graph, a valid solution without any obstacle violations can be obtained, as shown by the solid line example in Figure 7(c). Note that the solution on the OARSMT-guided sparse graph might not be able to be obtained on an ordinary sparse graph such as Figure 7(a). Besides, each net's additional grid lines are only applied for its own maze routing, so each

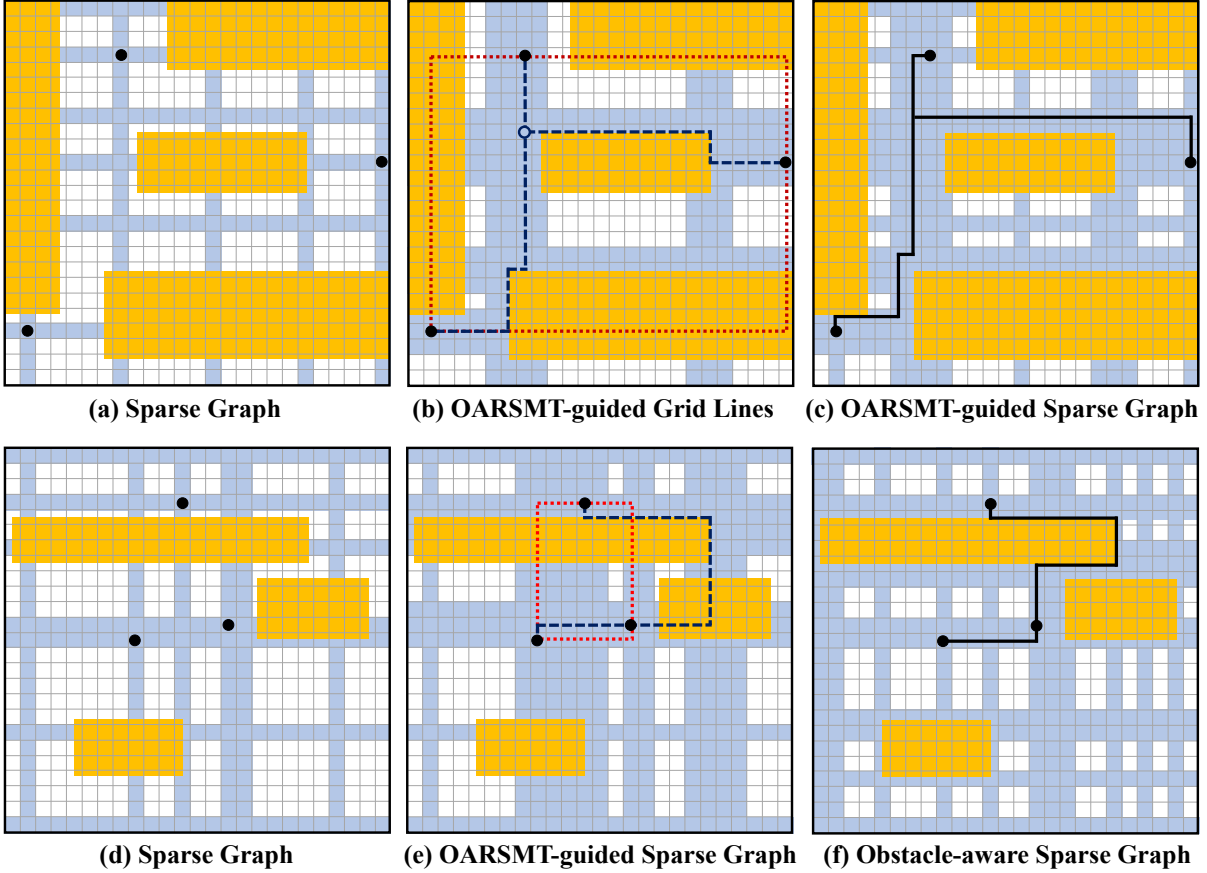
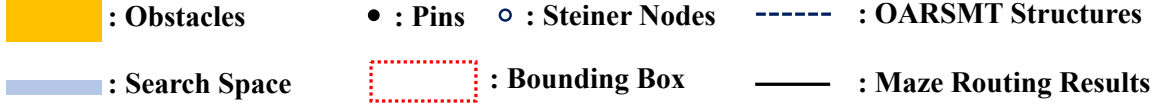


Figure 7: Example of OARSMT-guided sparse maze routing and obstacle-aware sparse maze routing.

OARSMT-guided sparse graph has a limited complexity increase than the ordinary one. As a result, the proposed method has comparable execution time with better quality than using the ordinary graph.

(2) *Obstacle-aware Sparse Maze Routing*: After utilizing OARSMT-guided sparse maze routing, the overflow and obstacle-violated nets experience a significant reduction; however, there are still some nets with obstacle violations. As shown by the dotted OARSMT in Figure 7(e), the OARSMT algorithm considers only obstacles within the bounding box during the tree generation stage, which may result in invalid solutions. To fix this problem, the obstacle-aware sparse maze routing can be applied exclusively to the remaining nets with violations. Utilizing the additional grid lines extending from the boundaries of all obstacles and pins for maze routing, by combining these lines with the ordinary sparse graph, obstacle-aware sparse graph can be created, as shown in Figure 7(e) and (f). The solid lines illustrate a solution for obstacle-aware sparse maze routing. This method ensures that most nets successfully navigate around obstacles. Although the presence of numerous obstacles can slow down the obstacle-aware sparse maze routing process, it is only applied to a limited number of remaining nets. As a result, the overall runtime for this step remains reasonable.

6 Evaluations

6.1 Experiment Setup

The experiments are conducted on a server with Intel Xeon Gold 6348 CPU. In the experiments of the OARSMT algorithm, there are two types of benchmarks: Randomized testcases and standard benchmarks. Each testcase in benchmarks contains one net to be test, which follows the regular evaluation process as previous OARSMT

works [11, 4, 21]. For randomized testcase generation, 3 factors are set: The number of pins and obstacles, and the obstacle density on the layout. Other parameters are randomly generated. Each setting is tested 50 times to get the average result. Besides, we also test all the standard benchmarks IND, RC, and RT [22] involved in the compared works [11, 4, 21]. $k_l = 5$ and $k_m = 2$ in the experiments. For OARSMT comparison, the advanced work proposed by Lin et al. [11], a recent work [21] and a traditional work [4] are involved, with works [11, 4] reproduced. Similar to recent work [12], our experiments also apply the algorithm in work [11] by 2D mode. The 2D mode of work [11] does not trim any key techniques in the 3D mode, and thus it still maintains the quality with faster speed. Besides, as the tree generation in regular global routing flow typically generate 2D trees, applying work [11] under 2D mode is able to perform the comparison under a complete global routing flow.

In the experiments of obstacle-avoiding global routing, the framework of global router CUGR2.0 [20] is adopted, where the proposed algorithms are implemented. We utilize the same metrics as applied in the ICCAD19 global routing competition [23], including wirelength, via count, congestion overflow cost and so on. Meanwhile, we also evaluate the obstacle violations, following the same calculation method as the overflow cost in the competition. ISPD24 contest [24] benchmark circuits were used in our experiments as it contains testcases from the regular size to the very large size. We set the macros in the benchmarks as obstacles for our experiments, of which the areas are forbidden to be crossed by wires at all layers. Besides, we also add 60 random obstacles on each testcase of the benchmarks as additional testcases.

6.2 OARSMT Comparisons on Randomized Testcases

The OARSMT algorithm is first tested and compared. During the OARSMT algorithm comparisons, all obstacles in the layout are considered, rather than only considering those in the net’s bounding box as the initial routing flow. In this case, there is no violation in the experiments of OARSMT algorithm itself.

The wirelength difference and speedup of the proposed algorithm is shown in Table 1, compared with advanced work [11]. In Table 1, each row stands for a setting of the number of pins, and each column stands for a setting of the number of obstacles. Each group contains 4 runtime results corresponding to different obstacle densities. One can notice that the proposed algorithm has $\sim 10x - 2700x$ speedup from small cases to large cases.

The absolute values of the runtime for the proposed algorithm are also tested, and are 0.63ms for small cases and only 0.19s for large cases. This not only shows the fast speed, but also proves the scalability.

Besides, Table 1 also shows the wirelength difference, and negative results mean that the proposed algorithm has a smaller wirelength. The wirelength difference ranges from -5.76% to 2.68% . It is shown that the proposed algorithm can also outperform work [11] in the wirelength for various cases, and the wirelength improvement is 1.14% on average. For relatively large designs, the proposed algorithm shows $>3\%$ wirelength improvement. The experiments indicate that the proposed algorithm has better wirelength for randomized testcases compared with the previous work, but also spends orders of shorter runtime.

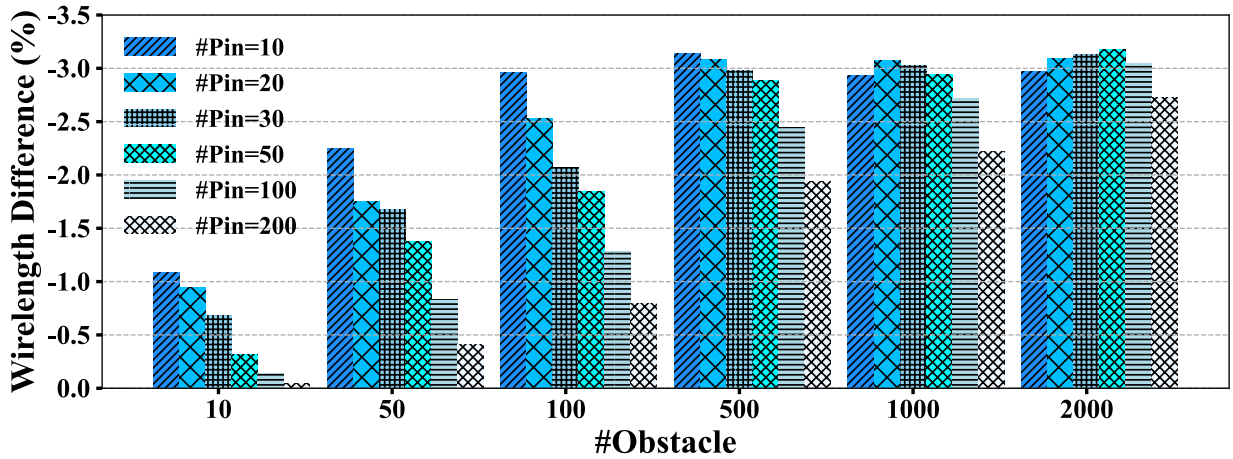


Figure 8: Wirelength improvement for rule enhancements

Moreover, we evaluate the wirelength improvement of the enhanced rules as shown in Figure 8, which shows the differences between the runs with and without using the enhanced rules. The algorithm with rule enhancements shows an average -1.88% wirelength improvement. For the cases with fewer pins ($\#pins \leq 30$) or a large number of obstacles ($\#obstacles \geq 500$), when obstacles each edge passes become complicated, it shows a bigger -2.22% and

Table 1: The comparisons with the advanced previous work [11] on the randomized testcases.

	Density	#Obs=10	#Obs=50	#Obs=100	#Obs=500	#Obs=1000	#Obs=2000
Speedup							
#Pin=10	10%	34.56x	57.03x	133.74x	965.18x	1709.18x	2711.79x
	30%	28.02x	42.13x	65.05x	436.41x	1037.00x	1255.36x
	50%	20.61x	23.86x	47.62x	277.52x	863.57x	1052.37x
	70%	19.97x	18.41x	31.61x	261.89x	949.72x	725.38x
#Pin=20	10%	50.07x	99.56x	143.85x	1073.18x	1713.21x	2332.41x
	30%	37.29x	63.26x	85.33x	402.39x	793.79x	1159.35x
	50%	37.37x	40.62x	55.80x	251.26x	501.56x	790.10x
	70%	37.41x	33.13x	45.35x	198.97x	361.32x	563.91x
#Pin=30	10%	174.33x	109.19x	179.57x	1075.40x	1718.38x	2443.06x
	30%	59.79x	72.72x	99.10x	420.68x	681.07x	763.08x
	50%	64.34x	54.72x	71.49x	256.15x	399.53x	643.97x
	70%	58.02x	43.52x	59.27x	166.03x	308.12x	493.75x
#Pin=50	10%	102.39x	157.40x	205.02x	1040.27x	1647.71x	1876.00x
	30%	114.99x	99.48x	135.85x	449.44x	602.45x	690.97x
	50%	112.97x	89.93x	100.86x	259.32x	380.30x	433.12x
	70%	106.00x	72.53x	81.37x	188.36x	267.95x	315.92x
#Pin=100	10%	206.47x	230.86x	282.12x	1073.62x	1656.79x	1916.65x
	30%	212.87x	185.91x	214.37x	492.41x	668.77x	619.63x
	50%	214.97x	168.15x	190.66x	338.00x	436.84x	441.54x
	70%	206.01x	151.89x	157.39x	252.90x	287.52x	261.67x
#Pin=200	10%	429.27x	383.08x	445.77x	1042.32x	1457.32x	1779.90x
	30%	398.38x	353.72x	372.01x	621.75x	757.48x	646.16x
	50%	389.05x	355.30x	352.46x	441.75x	521.98x	442.24x
	70%	342.13x	331.91x	310.92x	348.23x	378.06x	316.04x
Wirelength Difference (<0 Stands for Improvements)							
#Pin=10	10%	-2.51%	-2.42%	-2.81%	-5.00%	-4.26%	-5.76%
	30%	-0.76%	-1.68%	-2.89%	-4.65%	-4.44%	-4.54%
	50%	0.56%	-0.57%	-2.65%	-2.83%	-3.83%	-4.54%
	70%	-0.31%	-4.86%	-2.54%	-3.53%	-1.56%	0.53%
#Pin=20	10%	-1.46%	-1.53%	-1.83%	-3.40%	-3.50%	-4.47%
	30%	-0.27%	-0.89%	-1.73%	-2.69%	-3.84%	-4.48%
	50%	0.47%	0.72%	-0.29%	-2.00%	-2.96%	-3.86%
	70%	1.20%	-1.34%	-0.18%	-1.74%	-2.30%	-0.74%
#Pin=30	10%	-0.13%	-0.76%	-0.98%	-1.46%	-3.37%	-3.17%
	30%	0.37%	-0.04%	-0.50%	-1.33%	-2.91%	-2.38%
	50%	1.58%	1.46%	0.39%	-0.98%	-2.55%	-2.69%
	70%	1.77%	2.68%	2.14%	-0.01%	-3.53%	-3.58%
#Pin=50	10%	-1.29%	-1.02%	-1.36%	-2.29%	-3.18%	-3.47%
	30%	-0.85%	-0.22%	-0.19%	-2.08%	-3.21%	-3.79%
	50%	-0.61%	0.72%	-0.11%	-1.64%	-2.75%	-2.99%
	70%	-0.22%	1.89%	1.59%	-0.66%	-3.31%	-1.77%
#Pin=100	10%	-1.02%	-1.01%	-1.16%	-1.59%	-2.13%	-2.51%
	30%	-0.65%	-0.40%	-0.27%	-1.28%	-2.23%	-2.62%
	50%	-0.87%	0.57%	0.86%	-0.43%	-1.66%	-2.60%
	70%	-1.39%	1.29%	1.51%	-0.13%	-1.37%	-1.70%
#Pin=200	10%	-1.15%	-0.98%	-1.02%	-1.16%	-1.56%	-1.85%
	30%	-1.15%	-0.23%	-0.10%	-0.51%	-1.21%	-1.98%
	50%	-1.21%	-0.18%	0.35%	0.23%	-0.63%	-1.29%
	70%	-0.91%	-0.05%	1.03%	1.01%	0.06%	-0.92%

-2.69% wirelength improvement, respectively. The results prove that the rule enhancements, by exploring more design space, provide more opportunities to avoid local optimal solutions and achieve better wirelength.

Finally, we briefly report the wirelength and runtime comparisons with previous 2D OARSMT work [4]. The speedup of the proposed work compared to work [4] ranges from $\sim 11x$ - 7374x, with 1306x on average. Meanwhile, the wirelength difference ranges from -10.04% to -0.47%. The average wirelength improvement among all cases is 5.03%. The previous work [4] has a worse wirelength because it trims some optimized steiner nodes when building an initial tree structure at the early stages. This again indicates the advantages of the proposed algorithm on both quality and speed.

6.3 OARSMT Comparisons on Standard Benchmarks

Table 2: The comparisons on the standard benchmarks [22].

Test cases	#Pin/#Obs	Wirelength				Runtime (s)			
		[4]	GSLs [21]	(Lin et al.) [11]	Ours	[4]	GSLs [21]	(Lin et al.) [11]	Ours
IND1	10/32	0.6k	0.6k	0.6k	0.6k	0.08	0.01	0.01	0.0002
IND2	10/43	10.7k	9.5k	9.2k	9.7k	0.1	0.01	0.01	0.0041
IND3	10/50	0.7k	0.6k	0.6k	0.6k	0.18	0.01	0.01	0.0012
IND4	25/79	1.2k	1.1k	1.1k	1.2k	0.51	0.84	0.06	0.0042
IND5	33/71	1.4k	1.3k	1.4k	1.4k	0.41	0.57	0.02	0.0063
RC01	10/10	28.3k	26.0k	25.5k	26.1k	0.02	0.01	0.02	0.0070
RC02	30/10	44.5k	41.4k	41.0k	44.8k	0.03	0.04	0.04	0.0041
RC03	50/10	58.6k	54.2k	52.7k	60.7k	0.05	0.45	0.06	0.0089
RC04	70/10	63.7k	59.1k	56.2k	64.8k	0.08	0.48	0.11	0.0061
RC05	100/10	79.6k	74.1k	73.8k	78.9k	0.12	8.33	0.21	0.0065
RC06	100/500	86.1k	79.7k	78.7k	83.0k	27.14	462.88	7.57	0.0637
RC07	200/500	117.0k	108.8k	107.9k	113.7k	35.11	611.42	10.28	0.0623
RC08	200/800	122.4k	112.6k	111.3k	120.4k	94.38	475.22	34.34	0.1550
RC09	200/1000	120.4k	111.1k	110.2k	118.0k	151.69	604.82	48.18	0.1865
RC10	500/100	178.1k	164.4k	168.4k	169.0k	7.51	739.25	38.2	0.0540
RC11	1000/100	250.4k	232.5k	242.3k	234.3k	30.35	3260.22	23.57	0.2117
RC12	1000/10000	—	747.5k	—	749.7k	—	3398.36	—	0.2279
RT01	10/500	2.3k	2.1k	1.9k	2.3k	19.61	13.34	0.79	0.0247
RT02	50/500	50.3k	45.9k	45.0k	48.1k	24.29	23.11	5.69	0.0340
RT03	100/500	8.8k	8.0k	8.2k	8.3k	25.43	305.71	3.13	0.0437
RT04	100/1000	10.8k	9.7k	8.6k	12.1k	119.05	154.88	7.58	0.2569
RT05	200/2000	—	51.4k	45.2k	61.0k	—	622.37	82.12	0.4228
Total		1236.0k	1142.6k	1144.6k	1197.8k	536.16	6661.58	179.88	1.1410
Norm.		1.03	0.95	0.96	1.00	469.90	5838.37	157.65	1.00

- Each result of Lin et al. [11] is selected by the better one between the reproduction and [11]’s report; The results of GSLs [21] are referred from its report; The results of work [4] are from the reproduction as the benchmarks in its report are the old versions.
- The results with “—” cannot be obtained in neither 3 minutes nor the corresponding report. The total wirelength and runtime are only counted for the testcases that all 4 algorithms have results.

For OARSMT algorithms, besides the throughout randomized testcases and comparisons, we also compare the proposed algorithm on all standard benchmarks [22] adopted in the compared works, including the advanced work proposed by Lin et al. [11], the recent work GSLs [21], and the traditional work [4]. Each testcase is to generate one OARSMT for one net within a layout with obstacles. The results are shown in Table 2. The speedup of our work ranges from $\sim 150x$ to $5800x$, with trading limited wirelength overhead compared with the works [11, 21], and with even better wirelength compared with the work [4]. Note that for Lin et al. [11], there is no result for *RC12* in neither the reproduction nor its report, due to the large runtime. In contrast, the proposed algorithm only needs $\sim 0.2s$ for *RC12*. Besides, the runtime of the proposed algorithm also shows the scalability as it increases almost linearly with increasing the problem size, and this is in contrast with recent work GSLs [21]. In this case, with large amount of nets in complete designs, previous work can spend more time for tree generation than a traditional routing flow. In conclusion, the experiments on standard benchmarks also prove the high efficiency and scalability of the proposed algorithm. This is not only because of the theoretical lower time complexity, but also because of the simpler processing.

6.4 Proposed Obstacle-Avoiding Global Routing Evaluations

As shown in Table 3, we compare the proposed global router (“Ours”) with CUGR 2.0 [20], enhanced CUGR 2.0, and our global routing flow integrated with the advanced OARSMT [11] method (“Lin et al.”). The enhanced CUGR 2.0 is CUGR 2.0 with the increased edge cost for the obstacles during maze routing. The cost is large enough that can effectively make the maze routing avoid the obstacles in the sparse graphs if possible. We separately compare wirelength, via count, obstacle violation cost, congestion overflow cost and runtime. Note that the overflow cost does not include the obstacle violation cost.

In Table 3, CUGR 2.0 performs poorly in terms of obstacle violations. Although the enhanced CUGR 2.0 has shown significant improvement, it still fails to effectively eliminate obstacle violations. In contrast, the proposed global routing flow (“Ours”) can reduce the final obstacle violation to zero, which proves its effectiveness. Additionally,

Table 3: The comparisons with other global routers.

Benchmarks	Normalized Wirelength				Normalized Via Count				Normalized Overflow			
	CUGR 2.0	CUGR 2.0 Enhanced	(Lin et al.) [11]	Ours	CUGR 2.0	CUGR 2.0 Enhanced	(Lin et al.) [11]	Ours	CUGR 2.0	CUGR 2.0 Enhanced	(Lin et al.) [11]	Ours
ariane133_51	1.01	0.98	1.33	1.00	1.01	0.98	1.33	1.00	0.99	0.98	1.15	1.00
ariane133_68	1.05	0.98	2.00	1.00	1.05	0.98	2.69	1.00	0.99	0.98	1.10	1.00
nvdla	1.04	0.97	1.38	1.00	1.04	0.97	1.40	1.00	1.00	0.98	1.05	1.00
mempool_tile	1.00	0.98	0.77	1.00	1.00	0.98	0.77	1.00	0.99	0.98	0.77	1.00
bsg_chip	1.02	0.99	2.06	1.00	1.02	0.99	2.22	1.00	0.98	0.95	0.93	1.00
mempool_group	1.00	0.96	0.69	1.00	1.03	0.96	1.19	1.00	1.00	0.97	1.00	1.00
cluster	1.00	0.99	0.87	1.00	1.02	0.99	1.18	1.00	0.99	0.98	0.98	1.00
ariane133_51*	1.01	0.98	2.33	1.00	1.01	0.98	3.31	1.00	0.99	0.98	2.11	1.00
ariane133_68*	1.05	0.98	2.09	1.00	1.05	0.98	2.87	1.00	0.99	0.98	1.06	1.00
nvdla*	1.04	0.97	1.31	1.00	1.04	0.97	1.33	1.00	1.00	0.98	1.10	1.00
mempool_tile*	1.00	0.98	1.06	1.00	1.00	0.98	1.06	1.00	0.99	0.98	0.81	1.00
bsg_chip*	1.02	0.99	1.97	1.00	1.02	0.99	2.26	1.00	0.98	0.95	0.91	1.00
mempool_group*	1.00	0.96	0.69	1.00	1.03	0.96	1.19	1.00	0.99	0.97	0.99	1.00
cluster*	1.00	0.99	0.86	1.00	1.02	0.99	1.18	1.00	0.99	0.98	0.98	1.00
Average	1.02	0.98	1.39	1.00	1.02	0.98	1.71	1.00	0.99	0.97	1.07	1.00
Benchmarks	Obstacle Violation				Normalized Total Runtime							
	CUGR 2.0	CUGR 2.0 Enhanced	(Lin et al.) [11]	Ours	CUGR 2.0	CUGR 2.0 Enhanced	(Lin et al.) [11]	Ours				
ariane133_51	0.2k	0.2k	0	0	0.80	0.79	7.33	1.00				
ariane133_68	6.3k	5.7k	0	0	0.90	0.91	8.91	1.00				
nvdla	0.4k	0.2k	0	0	0.88	0.89	5.81	1.00				
mempool_tile	0.5k	0.5k	0	0	0.84	0.83	23.72	1.00				
bsg_chip	27.1k	25.1k	0	0	0.81	0.78	10.78	1.00				
mempool_group	1777.7k	3.9k	0	0	0.71	0.72	2.05	1.00				
cluster	2531.8k	9.5k	0	0	0.83	0.82	1.71	1.00				
ariane133_51*	0.2k	0.2k	0	0	0.79	1.05	8.61	1.00				
ariane133_68*	7.9k	7.1k	0	0	0.78	0.87	11.34	1.00				
nvdla*	0.4k	0.2k	0	0	0.77	0.89	5.75	1.00				
mempool_tile*	0.5k	0.5k	0	0	0.75	0.95	28.43	1.00				
bsg_chip*	25.1k	22.8k	0	0	0.90	1.07	11.00	1.00				
mempool_group*	1778.1k	3.8k	0	0	0.70	0.77	1.96	1.00				
cluster*	2559.9k	11.4k	0	0	0.81	0.79	1.53	1.00				
Average	622.57k	6.51k	0	0	0.81	0.87	9.21	1.00				

- The Lin et al. is our proposed obstacle-avoiding global routing flow with the advanced OARSMT [11].
- In the benchmark, cases without “*” represent obstacles that only include macro obstacles, while those with “*” include both macro obstacles and an additional 60 randomly generated obstacles.

“Ours” demonstrates reductions in wirelength and overflow in most test cases when compared to both the original and enhanced CUGR 2.0, achieving an average improvement of 1.96% in wirelength and a 28.06% reduction in overflow cost to enhanced CUGR 2.0, although with acceptable overhead in terms of count and runtime, as more detours are required to navigate around obstacles. The effectiveness of obstacle elimination and overflow is primarily due to the challenges posed by complex obstacle distributions. In traditional algorithms, treating obstacles similarly to overflow complicates the balancing of costs in each stage. This disrupts the collaboration of stages in a traditional global routing process. Meanwhile, maze routing sparse grids in traditional global routers without OARSMT guidance also limit the opportunities of avoiding obstacles. In this case, addressing obstacle violations directly in the early stage and modifying the later stages to incorporate early guidance allows global routing stages to effectively manage obstacles. This is also supported by the insights presented in Section 6.5.

Besides, to further evaluate the effectiveness of the proposed complete flow, we also replace the OARSMT algorithm in the proposed flow with the advanced OARSMT [11] (“Lin et al.” in Table 3). It shows that although both “Ours” and “Lin et al.” eliminate all obstacle violations in the benchmark, “Lin et al.” spends 9.21x runtime on average than “Ours”, with similar wirelength, via count, and overflow cost. This further demonstrates the efficiency of our obstacle-avoiding global routing flow with the proposed OARSMT algorithm.

6.5 Obstacle-Avoiding Global Routing Insight Analysis

Besides the results of the complete flow, we also analyze the insides, including runtime breakdown, the comparisons for initial routing step, the comparisons of using different graphs during maze routing, and the effectiveness of OARSMT-guided sparse maze routing

To further understand the runtime characteristics of the proposed global routing flow, we provide a detailed runtime breakdown analysis for each stage across different benchmarks. As shown in Figure 9, similar as transitional flows, the rip-up and reroute step consumes the largest portion of the runtime. Within this step, almost all the runtime is spent by

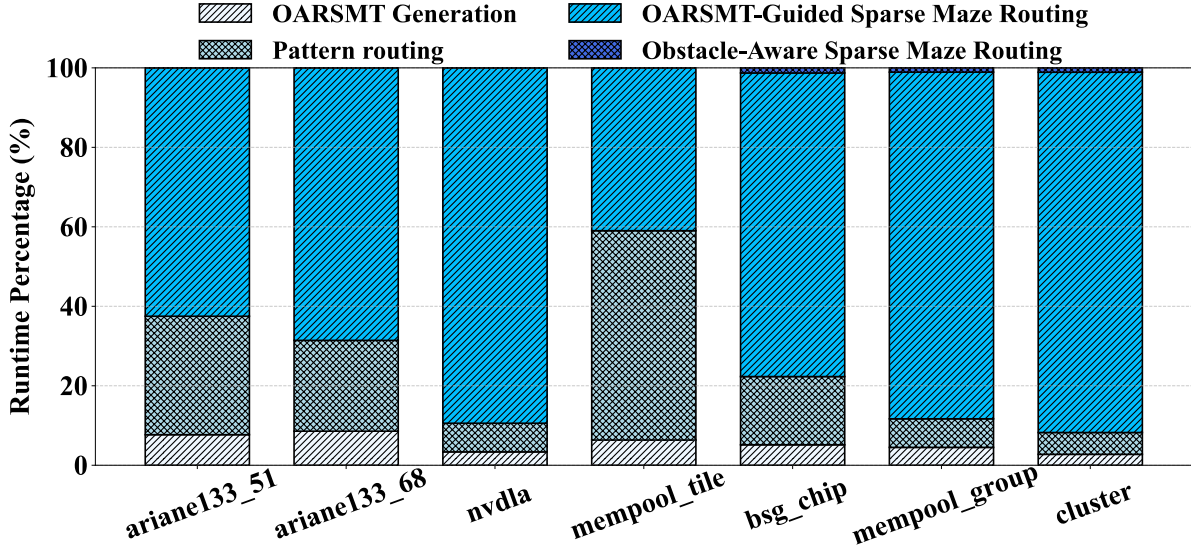


Figure 9: Runtime breakdown of the proposed flow across benchmarks, showing the percentage distribution of four stages: OARSMT generation, pattern routing, OARSMT-guided sparse maze routing, and obstacle-aware sparse maze routing.

OARSMT-guided sparse maze routing. In contrast, even for large cases, the final obstacle-aware sparse maze routing consumes no more than 0.14% of the total runtime in the worst-case scenario.

Next, Figure 10 illustrates the obstacle violations and runtime ratio of initial routing using the advanced OARSMT (“Lin et al.”) and our initial routing (“Ours”) to CUGR 2.0. Our initial routing has from 70% to 95% fewer obstacle violation cost than CUGR 2.0, from 16% to 71% fewer than “Lin et al.”. “Lin et al.” is unable to generate effective solutions in some cases, which results in a higher obstacle violation cost during the initial routing phase compared to “Ours”. Furthermore, “Ours” has $\sim 28x - 177x$ speedup compared with “Lin et al.”, with 149x on average. This again indicates the advantages of the proposed OARSMT algorithm on quality and speed towards complete designs.

Table 4: The comparison of normalized results of conventional maze routing with dense routing graphs to the proposed rip-up and reroute step, under the same initial routing flow. (Both methods have no obstacle violation)

Benchmark	Normalized Wirelength	Normalized Via Count	Normalized Overflow	Normalized Runtime
ariane133_51	0.998	1.001	1.16	66
ariane133_68	0.985	1.006	0.83	66
nvdla	0.996	1.038	0.85	87
mempool_tile	0.999	1.005	0.90	55
bsg_chip	0.994	1.012	0.46	76
mempool_group	0.999	1.248	0.86	77
cluster	-	-	-	Needs ≥ 4 Days
Average	0.995	1.052	0.84	71

Then, the comparisons between different rip-up and reroute approaches are analyzed. Table 4 shows the normalized metrics of conventional maze routing with dense routing graphs, compared to the proposed rip-up and reroute step, which includes OARSMT-guided sparse maze routing and obstacle-aware sparse maze routing. The initial routing steps both apply the proposed algorithms. It can be noticed that, although using dense routing graph in conventional maze routing can have better wirelength and overflow, it results in an average 71x increase in running time. For the second largest benchmark *mempool_group*, the proposed method requires approximately only one hour of runtime, whereas using conventional maze routing takes over 3 days. For the largest case *cluster*, the conventional maze routing cannot be finished in 4 days. Due to the large runtime particularly for complex cases, using dense graph for maze routing is impractical and the proposed approach is efficient.

Furthermore, we analyzed the effectiveness of OARSMT-guided sparse maze routing on obstacle violations and overflow. As shown in Figure 11, it illustrates the obstacle violations and overflow ratio of our obstacle-avoiding global routing

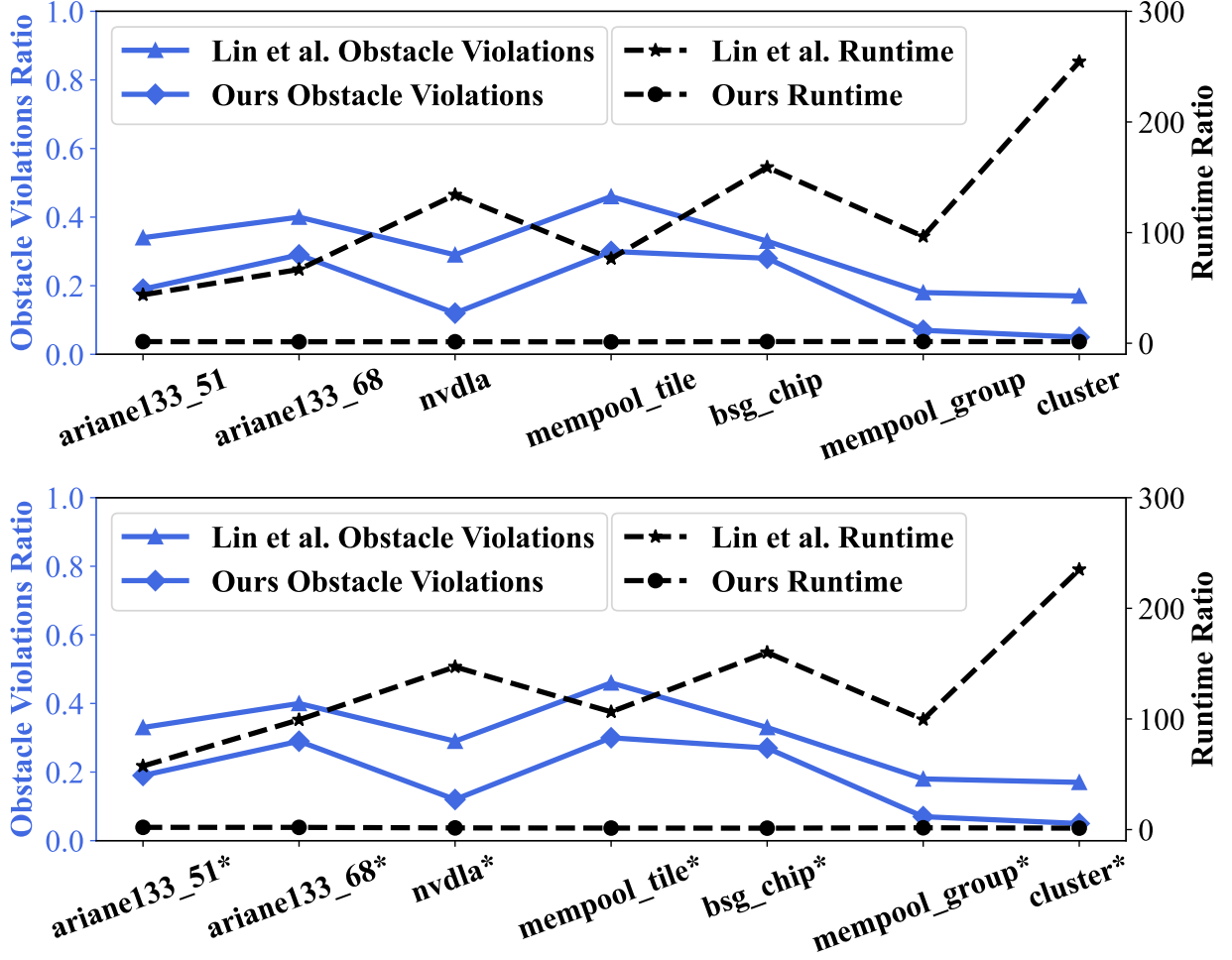


Figure 10: Obstacle violation and runtime ratio of the initial routing using the Lin et al. OARSMT and our initial routing to the CUGR 2.0. (The testcases with and without “*” are same meaning as those in Table 3.)

flow without the obstacle-aware sparse maze routing to the enhanced CUGR 2.0. Proposed OARSMT-guided sparse maze routing can completely eliminate obstacle violations in 4 cases. For the remaining 3 larger cases, although they are also almost cleared, which is significantly less than the enhanced CUGR 2.0. In addition to *mempool_tile*, our OARSMT-guided sparse maze routing outperforms the enhanced CUGR2.0 in all other cases, with the best improvement reaching 58.7% and the average improvement being 15.3%. The absolute value of the overflow cost for *mempool_tile* is only 13 less than the proposed flow. This proves that using the proposed OARSMT algorithm to consider the obstacles in the early stage, and providing the guidance for maze routing, the efficiency of avoiding the obstacles in for rip-up and reroute can be improved.

7 Conclusion

This work proposes an effective obstacle-avoiding global routing. Leveraging the proposed rule-based OARSMT algorithm in initial routing, it significantly reduces the obstacle violations in the early stage. By proposing the OARSMT-guided sparse maze routing and obstacle-aware sparse maze routing in rip-up and reroute, the obstacle violations are effectively eliminated. Compared with the advanced OARSMT algorithm, traded with limited wirelength overhead, the proposed OARSMT algorithm has $\sim 10x$ - $2700x$ and $\sim 150x$ - $5800x$ runtime speedup under randomized testcases and standard benchmarks, respectively. Compared with the enhanced advanced global router CUGR 2.0, proposed obstacle-avoiding global router successfully eliminates obstacle violations, and reduces wirelength and overflow cost on the modified ISPD 2024 benchmarks, traded limited via counts and runtime overhead. Besides, it achieves an average improvement of 1.96% in wirelength and a 28.06% reduction in overflow cost.

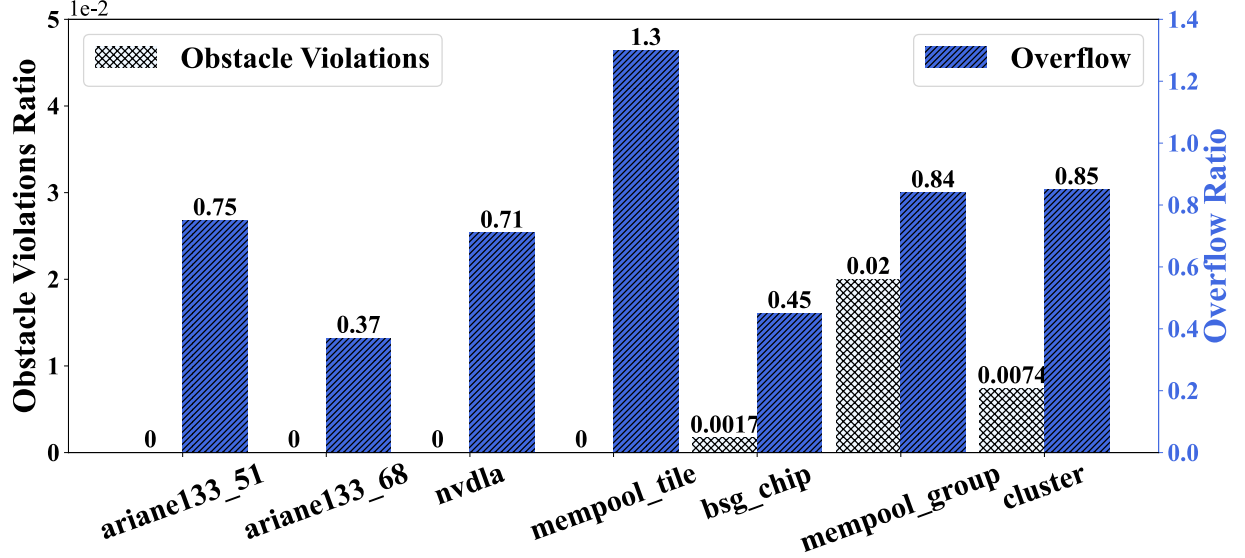


Figure 11: Obstacle violation and overflow ratio of the proposed flow after OARSMT-guided sparse maze routing to the enhanced CUGR 2.0.

References

- [1] Chris Chu and Yiu-Chung Wong. FLUTE: Fast Lookup Table Based Rectilinear Steiner Minimal Tree Algorithm for VLSI Design. *IEEE Transactions on Computer-Aided Design of Integrated Circuits and Systems*, 27(1):70–83, 2008.
- [2] K. Clarkson, S. Kapoor, and P. Vaidya. Rectilinear Shortest Paths through Polygonal Obstacles in $O(n(\log n)^2)$ Time. *Symposium on Computational Geometry*, pages 251–257, 1987.
- [3] Yang Yang, Qi Zhu, Tong Jing, Xianlong Hong, and Yin Wang. Rectilinear Steiner Minimal Tree Among Obstacles. *International Conference on ASIC*, 1:348–351, 2003.
- [4] Chung-Wei Lin, Szu-Yu Chen, Chi-Feng Li, Yao-Wen Chang, and Chia-Lin Yang. Obstacle-Avoiding Rectilinear Steiner Tree Construction Based on Spanning Graphs. *IEEE Transactions on Computer-Aided Design of Integrated Circuits and Systems*, 27(4):643–653, 2008.
- [5] Gaurav Ajwani, Chris Chu, and Wai-Kei Mak. FOARS: FLUTE Based Obstacle-Avoiding Rectilinear Steiner Tree Construction. *IEEE Transactions on Computer-Aided Design of Integrated Circuits and Systems*, 30(2):194–204, 2011.
- [6] Zhe Feng, Yu Hu, Tong Jing, Xianlong Hong, Xiaodong Hu, and Guiying Yan. An $O(N \log n)$ Algorithm for Obstacle-Avoiding Routing Tree Construction in the λ -Geometry Plane. *International Symposium on Physical Design*, pages 48–55, 2006.
- [7] Chung-Wei Lin, Shih-Lun Huang, Kai-Chi Hsu, Meng-Xiang Lee, and Yao-Wen Chang. Multilayer Obstacle-Avoiding Rectilinear Steiner Tree Construction Based on Spanning Graphs. *IEEE Transactions on Computer-Aided Design of Integrated Circuits and Systems*, 27(11):2007–2016, 2008.
- [8] Prasun Ghosal, Arindam Das, and Satrajit Das. Obstacle Aware RMST Generation Using Non-Manhattan Routing for 3D ICs. *Advances in Computing and Information Technology*, pages 657–666, 2013.
- [9] Prasun Ghosal, Satrajit Das, and Arindam Das. A Novel Algorithm for Obstacle Aware RMST Construction during Routing in 3D ICs. *Advances in Computing and Information Technology*, pages 649–658, 2013.
- [10] Chih-Hung Liu, Chun-Xun Lin, I-Che Chen, D. T. Lee, and Ting-Chi Wang. Efficient Multilayer Obstacle-Avoiding Rectilinear Steiner Tree Construction Based on Geometric Reduction. *IEEE Transactions on Computer-Aided Design of Integrated Circuits and Systems*, 33(12):1928–1941, 2014.
- [11] Kuen-Wey Lin, Yeh-Sheng Lin, Yih-Lang Li, and Rung-Bin Lin. A Maze Routing-Based Methodology With Bounded Exploration and Path-Assessed Retracing for Constrained Multilayer Obstacle-Avoiding Rectilinear Steiner Tree Construction. *ACM Transactions on Design Automation of Electronic Systems*, 23(4):1–26, 2018.

- [12] Po-Yan Chen, Bing-Ting Ke, Tai-Cheng Lee, I-Ching Tsai, Tai-Wei Kung, Li-Yi Lin, En-Cheng Liu, Yun-Chih Chang, Yih-Lang Li, and Mango C.-T. Chao. A Reinforcement Learning Agent for Obstacle-Avoiding Rectilinear Steiner Tree Construction. *International Symposium on Physical Design*, page 107–115, 2022.
- [13] Min Pan and Chris Chu. FastRoute: A Step to Integrate Global Routing into Placement. *IEEE/ACM International Conference on Computer Aided Design*, pages 464–471, 2006.
- [14] Yue Xu, Yanheng Zhang, and Chris Chu. FastRoute 4.0: Global Router with Efficient Via Minimization. *Asia and South Pacific Design Automation Conference*, pages 576–581, 2009.
- [15] Jhih-Rong Gao, Pei-Ci Wu, and Ting-Chi Wang. A New Global Router for Modern Designs. *Asia and South Pacific Design Automation Conference*, pages 232–237, 2008.
- [16] Yen-Jung Chang, Yu-Ting Lee, and Ting-Chi Wang. NTHU-Route 2.0: A Fast and Stable Global Router. *IEEE/ACM International Conference on Computer-Aided Design*, pages 338–343, 2008.
- [17] Jarrod A. Roy and Igor L. Markov. High-Performance Routing at the Nanometer Scale. *IEEE Transactions on Computer-Aided Design of Integrated Circuits and Systems*, 27(6):1066–1077, 2008.
- [18] Tai-Hsuan Wu, Azadeh Davoodi, and Jeffrey T. Linderth. GRIP: Scalable 3D Global Routing Using Integer Programming. *ACM/IEEE Design Automation Conference*, pages 320–325, 2009.
- [19] Yue Xu and Chris Chu. MGR: Multi-Level Global Router. *IEEE/ACM International Conference on Computer-Aided Design*, pages 250–255, 2011.
- [20] Jinwei Liu and Evangeline F.Y. Young. EDGE: Efficient DAG-based Global Routing Engine. *ACM/IEEE Design Automation Conference*, pages 1–6, 2023.
- [21] Tiancheng Zhang, Zhipeng Lü, and Junwen Ding. Guiding Solution Based Local Search for Obstacle-Avoiding Rectilinear Steiner Minimal Tree Problem. *IEEE Transactions on Emerging Topics in Computational Intelligence*, pages 1–14, 2023.
- [22] DIMACS Implementation Challenge in Collaboration with ICERM: Steiner Tree Problems. <https://dimacs11.zib.de/downloads.html>, 2016.
- [23] Sergei Dolgov, Alexander Volkov, Lutong Wang, and Bangqi Xu. 2019 CAD Contest: LEF/DEF Based Global Routing. *IEEE/ACM International Conference on Computer-Aided Design*, pages 1–4, 2019.
- [24] Rongjian Liang, Anthony Agnesina, Wen-Hao Liu, and Haoxing Ren. GPU/ML-Enhanced Large Scale Global Routing Contest. *International Symposium on Physical Design*, pages 123–130, 2024.